Scientific paper

Functionalization of Single Wall Carbon Nanotubes by Hydroxyethyl Cellulose

Svetlana Jovanović,[1] Zoran Marković,[1] Duška Kleut,[1] Nebojša Romčević,[2] Milena Marinović Cincović,[1] Miroslav Dramićanin[1] and Biljana Todorović Marković[1]

[1] *"Vinča" Institute of Nuclear Sciences, P.O.B. 522, 11001 Belgrade, Serbia*

[2] *Institute of Physics, P.O.B. 68, 11001 Belgrade, Serbia*

** Corresponding author: E-mail: biljatod@vinca.rs; Phone 381 11 2455 451, fax.381 11 3440100*

Received: 05-03-2009

Abstract

The results of synthesis and characterization of single wall carbon nanotubes functionalized by hydroxyethyl cellulose have been presented. The properties of pristine and modified single wall carbon nanotubes have been compared by different techniques: thermo-gravimetric analysis, Raman spectroscopy, Fourier transform infrared and UV-Vis-NIR spectroscopy. Raman analysis reveals that smaller amount of hydroxyethyl cellulose is required for functionalization of metallic single wall carbon nanotubes compared to semiconducting ones. FTIR analysis has shown the presence of hydroxyethyl groups which is strong evidence for nanotube modification.

Keywords: single wall carbon nanotubes; non-covalent functionalization; hydroxyethyl cellulose; Raman spectroscopy

1. Introduction

Due to their unique physical and chemical properties, single wall carbon nanotubes (SWCNTs) discovered by Iijima in 1991[1], have attracted a great attention of many researchers.[2–5] They found numerous applications in electronics such as field emission displays, diodes and transistors, sensors etc. Many carbon-based compounds (fullerenes) with different biological targets have been synthesized, displaying a range of biological activities potentially useful in anticancer or antimicrobial therapy, cytoprotection, enzyme inhibition, controlled drug delivery and contrast- or radioactivity-based diagnostic imaging.[6,7] Thus, biological applications of nanotubes could be very interesting but low solubility of nanotubes might be a problem.[8,9] Moreover nanotubes are difficult to suspend in water. They easily aggregate because of substantial van der Waals interactions between them.[10] Lack of solubility has imposed great limitations to the use of SWCNTs. It is possible to improve solubility by applying chemical methods such as covalent modification of SWCNTs[11] and sidewall functionalization.[12] Main disadvantage of covalent modification is that attached chemical groups cause changes in physical properties of SWCNTs. In this way, non-covalent procedures are desirable for dispersion of carbon nanotubes because they can maintain their own structure and electronic properties, which should be free from the presence of extensive covalent type chemical functionalization.[13]

Due to their abilities to bind cells and across the cell membrane, functionalized SWCNTs can be used as a nanovector for drug delivery and phototherapy.[14,15] Saito et al. demonstrated that multiwall carbon nanotubes (MWCNTs) have good bone-tissue compatibility, permit regeneration of broken bone and closely integrated with bone tissue.[16] In recent studies, SWCNTs have been used as an antibacterial agent due to their ability to absorb bacteria.[17] The SWCNTs as well as multiwall carbon nanotubes could be functionalized with biological active molecule and biological species including carbohydrates, amino acids, peptides and nucleic acids.[18–20]

In this study we chose hydroxyethyl cellulose (HEC) to non-covalently functionalize the SWCNTs because several controlled drug release formulas are deve-

loped on the base of HEC as drug matrix and due to the reinforcement and protection of carbon nanotubes (CNTs), cotton textiles exhibit enhanced mechanical properties, extraordinary flame retardancy, improved UV-blocking and super water repellent properties.[21,22] The HEC is a nonionic cellulose derivative with hydroxyethyl groups attached to the polymer. Hydroxyethyl groups attach to the OH groups of the structure by ether linkages.[23] A high degree of substitution (from 1.5 to 2.5 out of 3 maximum) gives HEC superior solubility in water and various brines.[24]

2. Experimental

2. 1. Materials

Purified SWCNTs (diameter 5 nm, length 4 μm, purity >95%) were purchased from BuckyUSA. The surfactant-HEC (SE Tylose GmBH&Co KG Wiesbaden, Germany) was used as received.[24]

2. 2. Preparation of dispersion of SWCNTs

A stock solution containing 20 mg of HEC in 100 ml distilled/deionized water was made up, respectively. A dispersion of pristine SWCNTs in tetrahydrofurane (THF) was ultrasonicated for comparing to functionalized ones. An amount of 25 mg of as-prepared SWCNTs was added to 100 mL to the stock solutions. The SWCNT solutions were sonicated (ultrasonic bath with power 750 W) for 3 hours. After sonication, all samples were centrifuged with Sigma, 2–16 at 4000 rpm (rcf = 2575 x g) for 1 h. For each sample the well-dispersed supernatant was taken for characterization leaving behind the precipitate.

The concentration of nanotube dispersion was determined by gravimetric method: 10 ml of nanotube dispersions was dried at 60 °C in air and the mass was measured. The obtained concentration was 40 mg/L.

2. 3. Characterization of Dispersion

2. 3. 1. Thermo-gravimetric Analysis

The thermal stabilities of pristine SWCNTs, HEC and SWCNTs/HEC dispersion were investigated by non-isothermal thermo-gravimetric analysis (TGA) and differential thermal analysis (DTA), using a SETARAM SETSYS Evolution-1750 instrument. SWCNTs/HEC dispersion was dried at room temperature in air. The measurements were conducted at a heating rate of 10 °C/min in a dynamic argon atmosphere (flow rate 20 cm^3/min) in the temperature range from 30 to 700 °C.

2. 3. 2. UV-Vis-NIR Spectroscopy

UV-Vis-NIR spectra were recorded at room temperature in a Brand disposable plastic UV cuvette with thickness of 10 mm using the Fiber optics UV-Vis-NIR AVANTES spectrophotometer.

2. 3. 3. Fourier Transform Infrared Spectroscopy

For the Fourier transform infrared (FTIR) spectroscopy analysis, nanotube dispersion was dried at temperature of 60 °C. Pristine and dried modified nanotubes as well as HEC were mixed with KBr powder and pellets were formed. FTIR spectra were measured at room temperature in the spectral range from 400 to 4000 cm^{-1}, on a Nicollet 380 FT-IR, Thermo Electron Corporation spectrometer.

2. 3. 4. Raman Spectroscopy

Raman spectra of pristine and modified SWCNTs were obtained by Micro Raman Chromex 2000 and JY 1000 Raman system using 532 nm of a frequency doubled Nd:YaG laser and 647 nm from Ar ion laser with power of 2mW, respectively. The spectral resolutions were 4 and 0.2 cm^{-1}, respectively. Samples of pristine and dried modified nanotubes were pressed in the shallow hole of indium substrate.

2. 3. 5. Verification of Stabilization Mechanism

In order to check the stabilization mechanism of SWCNTs/HEC dispersion we added 10 mg/L, 50 mg/L, 100 mg/L and 1000 mg/L NaCl to 25 ml of SWCNTs/HEC dispersion, respectively.

3. Results and Discussion

3. 1. Thermo-gravimetric Analysis

The thermo-gravimetric analysis (TGA) of pristine and functionalized SWCNTs as well as HEC is presented in Fig.1a. TGA of prepared SWCNTs/HEC sample was studied to understand the details of its decomposition process and to know the thermal stability of prepared SWCNTs/HEC specimen. Thermal degradation of SWCNTs/HEC consists of two main phases. As can be seen from Fig. 1a, the initial weight loss of 5.58% (up to 200 °C) is due to the evaporation of physically adsorbed water. The subsequent loss of 46.86 % (200–800 °C) is due to the decomposition of hydroxyethyl cellulose.

3. 2. UV-Vis-NIR Spectroscopy

In Fig. 1b, UV-Vis- NIR spectra of HEC and modified SWCNTs are presented. As for HEC itself one could observe three peaks at 216, 217 and 220 nm, respectively. As for functionalized SWCNTs, the broad peak observed at 254 nm is due to dispersed and non-bundled

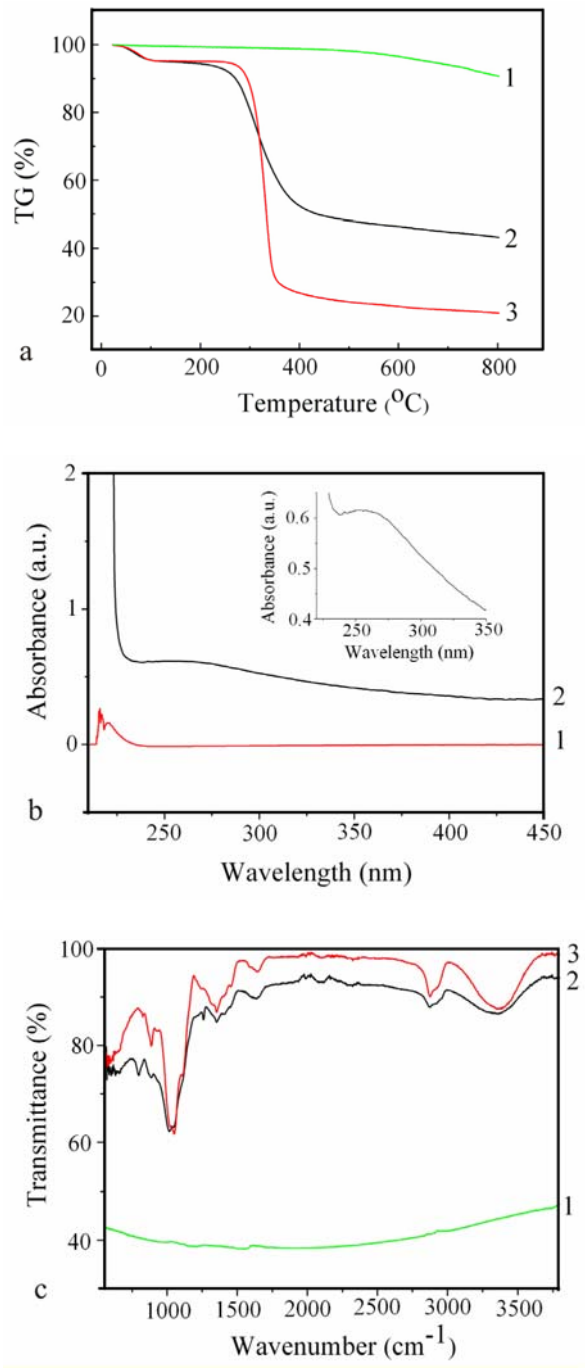

Fig. 1. (a) TGA curves of 1) pristine SWCNTs, 2) dried SWCNTs modified by HEC and 3) HEC, (b) UV/Vis NIR spectra of HEC 1), SWCNTs modified by HEC 2) as well as magnified SWCNTs/HEC spectrum in the upper right corner (c) FTIR spectra of pristine nanotubes (curve 1), dried SWCNTs modified by HEC (curve 2) and HEC (curve 3).

SWCNTs.[25] The most prominent peak observed at 254 nm of SWCNTs/HEC spectra is magnified and shown in the upper right corner of Fig. 1b. This indicates the presence of carbon nanotubes dispersed by HEC in the solvent.

3. 3. FTIR Spectroscopy

The FTIR spectra of pristine SWCNTs, functionalized SWCNTs and HEC in the region from 400–4000 cm^{-1} are presented in Fig. 1c. Curve 1 shows peaks at 1607 cm^{-1} which stem from aromatic C=C stretching bonds as well as 2850 and 2920 cm^{-1} which from C-H bonds.[26,27] Curves 2 and 3 show peaks at 1015 and 1260 cm^{-1} which stem from hydroxyl groups as well as broad bands at 1600 and 3300cm^{-1}.[27] Also, curves 2 and 3 show peak at 790 cm^{-1} and broad bands at 1350 and 2900 cm^{-1} which originate from ethyl groups.[28] Based on the presented FTIR spectra we could conclude that there was a good agreement of FTIR spectra of HEC–Fig. 1c (curve 3) and functionalized SWCNTs-Fig. 1c (curve 2). Therefore, these results could indicate successful functionalization of SWCNTs by HEC.

3. 4. Raman Spectroscopy

Resonance Raman spectroscopy has played an important role in the characterization of carbon nanotubes, both in terms of the diameter distribution in single wall carbon nanotube bundles and whether a nanotube is metallic or semiconducting.[29] In Fig. 2a, Raman spectra of pristine and modified SWCNTs by hydroxylethyl cellulose are presented. The peaks stem from nanotubes has been found at 155, 268, 1350, 1590 and 2625 cm^{-1}. The most intense feature is the G-band at 1590 cm^{-1} which is associated with several tangential C-C stretching transitions of the single wall carbon atoms. The peak at 1350 cm^{-1} is usually called D-band, which is associated with the vibration of sp^3-bonded carbon atoms existed at the defects in the hexagonal graphitic layers. G'-band at 2625 cm^{-1} is a second-order related harmonic.[30] The G'-band is an intrinsic property of the nanotube and the graphite, and present even in defect-free nanotubes for which the D band is completely absent.

Raman active radial breathing mode (RBM) of pristine SWCNTs and SWCNTs/HEC observed in range from 100 to 300 cm^{-1} is presented in Fig. 2b. In this mode, all carbon atoms are moving in-phase in the radial direction. For 532 nm excitation, RBM signals in the regions of 130–150, 150–215 and 230–300 cm^{-1} originate from the van Hove electronic transitions of semiconducting single wall carbon nanotubes (s-SWCNT-E_{44}^{s}, s-SWCNT-E_{33}^{s}) and metallic single wall carbon nanotubes (m-SWCNT-E_{11}^{m}), respectively. As a result, relative content of m- and s- SWCNTs before and after functionalization in this region can be evaluated from the resonant Raman spectra. Ratio of semiconducting to metallic nanotubes after treatment was determined in accordance with procedure developed earlier.[31] Distributions of semiconducting and metallic nanotubes are fitted with two Lorentzians. Relative quantity of semiconducting and metallic nanotubes after functionalization was determined by dividing the areas of

the Lorentzians by the areas of corresponding Lorentzians of pristine nanotubes. Mean diameters of semiconducting and metallic nanotubes were determined from central positions of Lorentzians, using relations between nanotube diameter and RBM frequency.

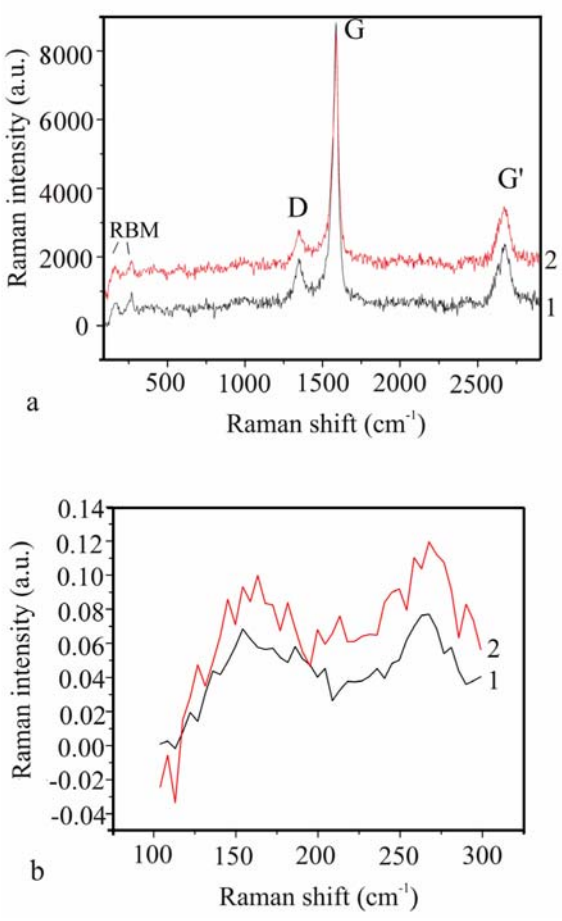

Fig. 2. (a) Raman spectra of pristine (1) and modified SWCNTs by HEC (2); (b) RBM spectra of pristine (1) and modified SWCNTs by HEC (2).

The important point about RBM band is the fact that the energy (wavenumber) of these vibration modes only depends on the diameter of SWCNTs. The ratio of the number of m-SWCNTs to number of s-SWCNTs in the observed samples, hereafter referred to the M:S ratio can be found by approximating the mean diameter distributions for m- and s-SWCNTs. Results of fitting procedure assuming that the ratio of metallic to semiconducting nanotubes is 1:2 are presented in Table 1.

Results in Table 1 indicate us that HEC interacts better with metallic nanotubes and mean diameter of functionalized metallic nanotubes is almost identical to pristine SWCNTs. It means that only few HEC molecules are necessary for functionalization of metallic nanotubes. For functionalization of s-SWCNTs, more HEC molecules are necessary which results in significantly larger mean diameter than that of pristine nanotubes.

During ultrasound treatment, cavities are formed on the surface of powder of nanotubes. Surface of powder is shocked with water bursts that remove smaller nanotubes first. Process is quite similar to removal of dirt in ultrasound cleaners where smaller particles are removed easier than larger. Since metallic nanotubes are thinner, they depart bundles easier than larger semiconducting nanotubes. Also due to size, smaller number of HEC molecules are required for suspension of lighter metallic SWCNTs than for heavier semiconducting SWCNTs.

Metallic and semiconducting SWCNTs have been found to exhibit different Raman lineshapes for the G-band. Early studies of ensemble of SWCNT indicate that laser radiation with energy 2.41 eV resonates dominantly with s-SWCNTs. Red and infrared laser excitations resonate better with m-SWCNTs.[32] Profile of G band of s-SWCNTs is composed of basically four Lorenzian components.[33] Raman spectra of m-SWCNTs exhibit only two strong peaks with Lorentzian and Breit Wigner Fano line shapes.[34]

To track changes in the G band positions and width we have carried out lineshape analysis designed to minimize the number of independent fitting parameters. The intensity of all peaks was normalized to yield the same intensity for the G band at 1590 cm^{-1}. In the case of pristine nanotubes, we have fitted the region from 1500–1750 cm^{-1} with the sum of four Lorentzian components. As for modified nanotubes, the region from 1500–1750 cm^{-1} has been fitted with the sum of two Lorentzian functions. In Fig. 3, fitted Raman spectra of G- band of pristine and modified SWCNTs are presented. As could be observed in Fig. 3a, four components with peaks at 1533, 1565, 1587 and 1602 cm^{-1} could be identified.

The intensity of components at 1533 and 1602 cm^{-1} is very small. After nanotube functionalization, only two

Table 1. The positions of G^- and G^+-band, the enrichment factors of m- and s-SWCNTs and mean diameters of nanotubes in these fractions at E_{laser} = 2.41 eV.

	G^- (cm^{-1})	G^+ (cm^{-1})	s-SWCNTs (%)	m-SWCNTs (%)	$\bar{d}_{s\text{-SWCNTs}}$ (nm)	$\bar{d}_{m\text{-SWCNTs}}$ (nm)
pristine SWCNTs	1565.15± 3.99	1587.88± 0.36	67.0	33.0	1.65± 0.01	0.98± 0.01
SWCNTs/ HEC	1571.76± 4.67	1589.72± 0.59	54.6	45.4	1.70± 0.04	0.98± 0.02

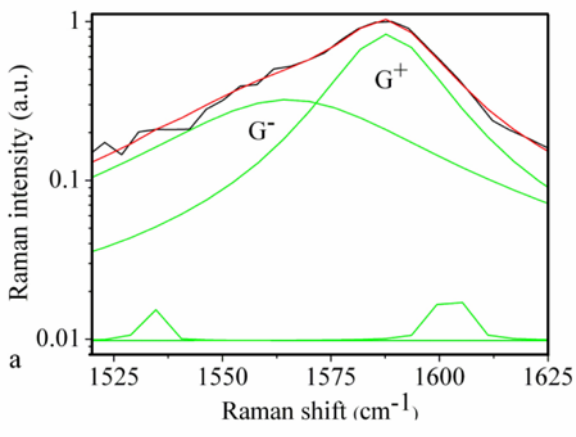

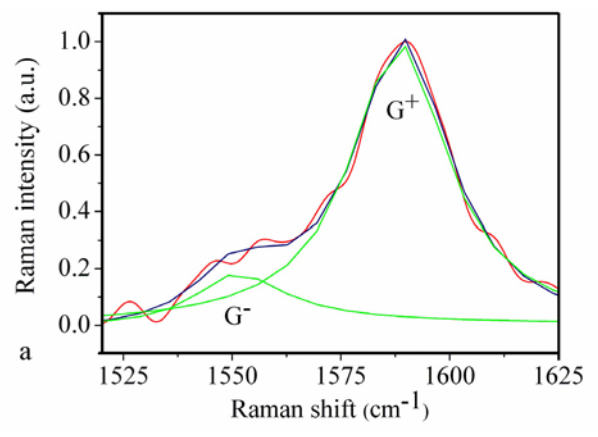

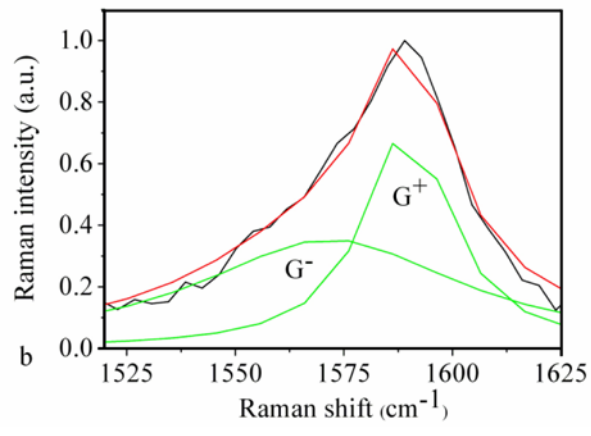

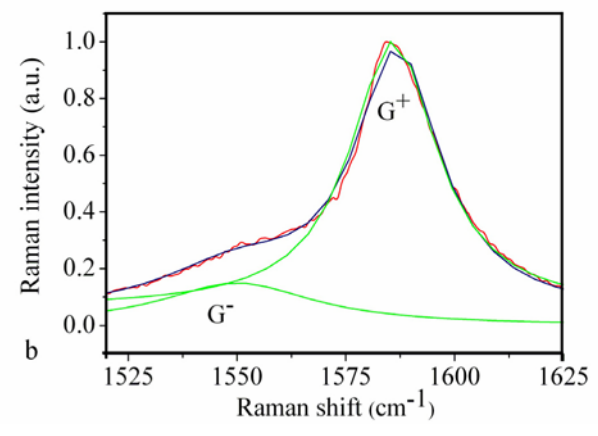

Fig. 3. Deconvoluted Raman spectra of pristine (a) and modified SWCNTs by HEC (b). E_{laser} = 2.41 eV.

Fig. 4. Deconvoluted Raman spectra of pristine (a) and modified SWCNTs by HEC (b). E_{laser} = 1.91 eV.

peaks (G^- and G^+) could be identified. Recently, Husanu et al showed that only two G-peaks could be observed in Raman spectra after nanotube functionalization because nanotubes were debundled.[35] The G^+-feature is associated with carbon atom vibrations along nanotube axis (LO phonon mode) and its frequency ω_{G+} is sensitive to charge transfer from dopant additions to SWCNTs.[36] The G^--feature is associated with vibrations of carbon atoms along circumferential direction of the SWCNTs (TO phonon) and its lineshape is highly sensitive to whether the SWCNTs is metallic or semiconducting.

After HEC processing, we have found that position of G^- and G^+ band components are shifted several cm^{-1}. G^- peak of SWCNTs/HEC is upshifted 6 cm^{-1}, while G^+ peak is downshifted 2 cm^{-1}. Previous Raman studies of modified SWCNTs have shown that removing electrons from SWCNTs results in a downshift of the G^+-band peak as observed here.[36] In fact, G^+-band downshift is probably associated with electron transfers from nanotube to glucose unit of HEC.

In order to investigate the vibrational properties of metallic SWCNTs, Raman spectra of pristine and modified nanotubes were measured by red laser with energy of 1.91 eV as well. In Fig. 4, deconvoluted Raman spectra of G band of pristine and modified nanotubes are presented. The spectra were fitted by the sum of Breit-Wigner-Fano (BWF) and Lorentzian functions. The lower frequency G^--modes from metallic tubes were fitted by applying BWF function, while the G^+-mode for semiconducting tubes was fitted by Lorentzian function, in accordance with resonance Raman studies on isolated SWCNTs.[32]

Charge transfer to SWCNTs can lead to an intensity increase or decrease of the BWF feature.[36] As can be seen from Fig. 4, the intensity of BWF feature of functionalized nanotubes decreases. The decrease of BWF contribution occurred as a consequence of the decrease in electronic density and therefore of the electron-phonon coupling effect in metallic nanotubes. In fact, it has been suggested that the plasmon coupling between tubes controls the intensity of the BWF contribution to the G-band for metallic tubes controls the intensity of the BWF contribution to the G-band for metallic tubes.[37]

Based on data presented in the diagram that relates positions of BWF and Lorentzian with nanotube diameter, the mean diameters of metallic and semiconducting SWCNTs were calculated and listed in Table 2.[38]

Table 2. The positions of G^- and G^+ bands and mean diameters of s-SWCNTs and m-SWCNTs. The laser energy was 1.91 eV.

	$G^-(cm^{-1})$	$G^+(cm^{-1})$	$\bar{d}_{s\text{-}SWCNTs}$ (nm)	$\bar{d}_{m\text{-}SWCNTs}$ (nm)
Pristine SWCNTs	1550.01±0.95	1589.23±0.13	1.37±0.08	1.09±0
SWCNTs/HEC	1550.01±0.42	1586.90±0.05	1.49±0.08	1.09±0

Concerning the values of mean diameters of pristine and modified SWCNTs, we concluded that HEC disperses metallic SWCNTs better than semiconducting ones. There is a difference between values of diameter obtained from RBM and G Raman spectra because both methods of diameter calculation depend on literature results that are not quite conclusive.

3. 5. The Stabilization Mechanism of Prepared SWCNTs

The SWCNTs were sonicated in HEC aqueous medium. During ultrasonication, the surfactant adsorbed on nanotube surface may cause the exfoliation of nanotube by steric[39] and electrostatic[40] repulsions. The ultrasonication treatment provided local high shear especially at the end of bundle.[41] When gaps formed at the bundle end, the surfactant could be absorbed and caused the separation of the single nanotube from the bundle.[42]

The HEC belongs to group of the nonionic polymeric surfactants. It differs from plain or regular cellulose so that some or all of the hydroxyl groups of the glucose repeat unit have been replaced with hydroxyethyl ether groups.[24] These hydroxyethyl groups get in the way when the polymer tries to . Because it cannot crystallize, HEC is soluble in water.

In previous studies concerning nanotube stabilization mechanism it was established that polymer was wrapped around nanotubes.[41,43] The possible mechanism of stabilization of SWCNTs by HEC is presented in Fig. 5. We assumed that glucose repeat units were adsorbed on sidewall defects of SWCNTs while ethyl groups were wrapped around carbon skeleton. Van der Waals interaction between hydrophobic moieties of polymer and sidewall SWCNTs were accomplished.[14,41] The length of hydroxyethyl groups was not long enough to wrap around whole nanotube but only partially. Our estimate of linear dimension of hydrophobic moiety is 0.8 nm. HEC is slightly chiral molecule and the nanotubes with corresponding chirality could be functionalized.[44] This was a reason for low dispersion efficiency of SWCNTs by HEC.

We have assumed that the stabilization mechanism of SWCNTs by HEC was realized on two levels: the electrostatic stabilization and the steric. Electrostatic stabilization was caused by hydroxyl groups of HEC that were oriented to dispersion medium and made hydrogen bond with aqueous molecules. Steric stabilization was largely driven by repulsive steric force between adjacent hydroxyethyl groups bound to polymer chain.[39] The stabilizing

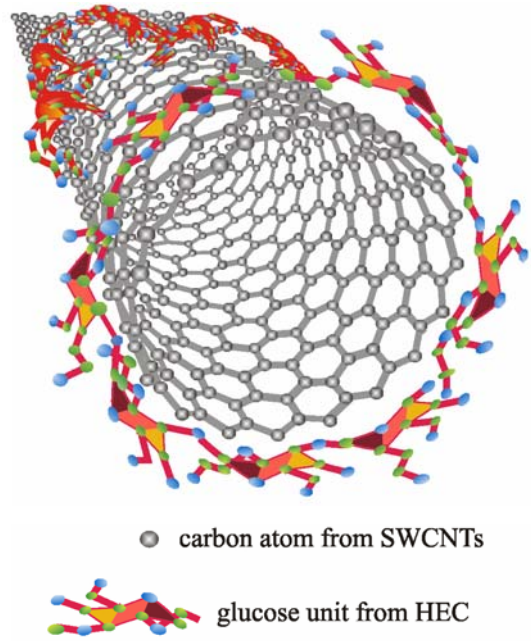

Fig. 5. Possible stabilization mechanism of SWCNTs using hydroxyethyl cellulose. Backbone of polymer HEC is wrapped around SWCNT due to absorption of glucose repeat units on the sidewall of SWCNT.

moieties that reach out into dispersion medium have to be mutually repulsive in order to effectively keep the particles at a distance from each other.

To check our presumptions about possible stabilization mechanism of SWCNTs/HEC dispersion, we added different amounts of NaCl to SWCNTs/HEC dispersion. In the case of exclusive ionic stabilization, adding the salt would cause precipitation of dispersion particles. On the other hand, particles stabilized sterically would not precipitate in the present of high concentration of salt. In our experiment, SWCNTs/HEC dispersion was stable for long time. Only small amount of SWCNTs/HEC precipitated after a few days. This result confirmed mechanism of stabilization through two levels of stabilization of carbon nanotubes.

4. Conclusion

In this paper, SWCNTs were functionalized by using nonionic surfactant hydroxyethyl cellulose. FTIR analysis has verified the presence of hydroxyl and ethyl groups in modified nanotube dispersions. Raman analysis reveals that smaller amount of hydroxyethyl cellulose is

required for functionalization of metallic SWCNTs compared to semiconducting ones. Stabilization mechanism of SWCNTs nanotubes by HEC was realized on two levels: steric and electrostatic.

5. Acknowledgements

This research was supported by the Ministry of Science of Republic of Serbia (project no. 145073).

6. References

1. S. Iijima, *Nature*, **1991**, *354,* 56–58.
2. M. S. Dresselhaus, G. Dresselhaus, P. C. Eklund, Science of Fullerenes and Carbon Nanotubes, Academic Press: San Diego, CA, **1996**.
3. R. Saito, G. Dresselhaus, M. S. Dresselhaus, Physical Properties of Nanotubes, Imperial College Press: London, **1998**.
4. F. Li, B. S. Cheng, G. Su, M. S. Dresselhaus, *Appl. Phys. Lett*. **2000,** *77*, 3161–3163.
5. B. W. Smith, Z. Benes, D. E. Luzzi, J. E. Fischer, D. A. Watters, M. J. Casavant, J. Schmidt, R. E. Smalley, *Appl. Phys. Lett.* **2000,** *77*, 663–665.
6. A. Isaković, Z. Marković, N. Nikolić, B. Todorović-Marković, S. Vranješ-Djurić, L. Harhaji, N. Raičević, N. Romčević, D. Vasiljević-Radović, M. Dramićanin, V. Trajković, *Biomaterials* **2006,** *27*, 5049–5058.
7. Z. Marković, B. Todorović-Marković, D. Kleut, N. Nikolić, S. Vranješ-Djurić, B. Babić-Stojić, M. Misirkić, Lj. Vučićević, K. Janjetović, A. Isaković, Lj. Harhaji, M. Dramićanin, V. Trajković, *Biomaterials* **2007,** *28*, 5737–5448.
8. M. Foldvari, M. Bagonluri, *Nanomed. Nanotechnol. Biol. Med*. **2008**, *4*, 173–200.
9. K. D. Ausman, R. Piner, O. Lourie, R. S. Ruoff, M. Korobov, *J. Phys. Chem. B* **2000,** *104* , 8911–8915.
10. A. P. Girifalco, M. Hodak, R. S. Lee, *Phys. Rev. B* **2000**, *62,* 13104–13110.
11. H. J. Eppley, H. L. Tsai, N. de Vries, K. Folting, G. Christou, D. N. Hendrickson, *J. Am. Chem. Soc.* **1995,** *117* , 301–317.
12. R. Sessoli, H. L. Tsai, A. R. Schake, S. Wang, B. J. Vincent, K. Folting, D. Gatteschi, G. Christou, D. H. Hendrickon, *J. Am. Chem. Soc*. **1993,** *115,* 1804–1816.
13. A. Hirsch, *Angew. Chem. Int. Ed*. **2002,** *41*, 1853–1859.
14. H. Dumortier, S. Lacotte, G. Pastorin, R. Marega, W. Wu, D. Bonifazi, J. P. Briand, M. Prato, S. Muller, A. Bianco, *Nano Lett*. **2006**, *6*, 1522–1528.
15. N. W. S. Kam, M. O'Connell, J. A. Wisdom, H. Dai, *Proc. Nat. Acad. Sci. U.S.A*. **2005**, *102,* 11600–11605.
16. Y. Usui, K. Aoki, N. Narita, N. Murakami, I. Nakamura, N. Ishigaki, H. Yamazaki, H. Horiuchi, H. Kato, S. Taruta, Y. A. Kim, M. Endo, N. Saito, *Small* **2008**, *4*, 240–246.
17. J. W. Kim, E. V. Shashkov, E. I. Galanzha, N. Kotagiri, V. P. Zharov, *Lasers Surg. Med*. **2007,** *39*, 622–634.
18. F. Pompeo, D. E. Resasco, *Nano Lett*. **2002**, *2*, 369–373.
19. V. Georgakilas, N. Tagmatarchis, D. Pantarotto, A. Bianco, J. P. Brianco, M. Prato, *Chem. Commun.* **2002,** *24***,** 3050–3051.
20. G. R. Dieckmann, A. B. Dalton, P. A. Johnson, J. Razal, J. Chen, G. M. Giordano, E. Munoz, I. H. Musselman, R. H. Baughman, R. K. Draper, *J. Am. Chem. Soc*. **2003,** *125*, 1770–1777.
21. K. S. V. Krishna Rao, M. S. C. Subha, B. Vijaya Kumar Naidu, M. Sairam, N. N. Mallikarjuna, T. M. Aminabhavi, *J. Appl. Polym. Sci*. **2006**, *102,* 5708–5718.
22. Y. Liu, X. Wang, K. Qi, J. H. Xin, *J. Mater. Chem*. **2008**, *18*, 3454–3460.
23. G. Marcelo, E. Saiz, M. P. Tarazona, *J. Chromatogr. A*, **2007**, *1165,* 45–51.
24. S. G. Cohen, H. C. Haas*, J. Am .Chem. Soc.*, **1950**, *72(9)*, 3954–3958.
25. L. Jiang, L. Gao, J. Sun, *J. Colloid Interface Sci*. **2003**, *260,* 89–94.
26. J. B. Kim, T. Premkumar, O. Giani, J. J. Robin, F. Schue, K. E. Geckeler, *Macromol. Rapid Commun*. **2007,** *28*, 767–771.
27. M. Baibarac, J. Baltag, S. Lefrant, J. Y. Mavellec, C. Bucur, *Diamond Relat. Mater*. **2008,** *17*, 1380–1388.
28. D. R. Lide, CRC Handbook of Chemistry and Physics, CRC Press **2003–2004**, pp.9–86–9–90.
29. M. S. Dresselhaus, G. Dresselhaus, A. Jorio, A. G. Souya Filho, M. A. Pimenta, R. Saito, *Acc. Chem. Res.* **2002**, *35*, 1070–1078.
30. C. G. Salzmann, B. T. T. Chu, G. Tobias, S. A. Llewellyn, M. L. H. Green, *Carbon,* **2007,** *45*, 907–912.
31. G. G. Samonidze, S. G. Chou, A. P. Santos, V. W. Brar, G. Dresselhaus, M. S. Dresselhaus, A. Selbst, A. K. Swan, M. S. Unlu, B. B. Goldberg, D. Chattopadhyay, S. N. Kim, F. Papadimitrakopoulos, *Appl. Phys. Lett*. **2004,** *85*, 1006–1008.
32. A. Jorio, A. G. Souza Filho, G. Dresselhaus, A. K. Swan, M. S. Unlu, B. B. Goldberg. M. A. Pimenta, J. H. Hafner, C. M. Lieber, R. Saito, *Phys. Rev B* **2002,** *65,* 1554121–1154129.
33. M. S. Dresselhaus, P.C. Eklund, *Adv. Phys*. **2000,** *49*, 705–814.
34. L. Alvarez, A. Righi, T. Guillard, S. Rols, E. Anglaret, D. Laplaze, J. L. Sauvajol, *Chem. Phys. Let.* **2000**, *316*, 186–190.
35. M. Husanu, M. Baibarac, I. Baltog, *Physica E* **2008,** *41*, 66–69.
36. M. S. Dresselhaus, G. Dresselhaus, R. Saito, A. Jorio, *Phys. Rep*. **2005,** *409*, 47–99.
37. P. Corio, A. Jorio, N. Demir, M. S. Dresselhaus, *Chem. Phys. Lett*. **2004**, *392*, 396–402.
38. M. Rasa, B. W. M. Kuipers, A. P. Philipse, *J. Colloid Interface Sci*. **2003,** *250*, 303–315.
39. R. S. Cohen, E. N. Roth, E. Baskaran, Y. L. Kalisman, I. Szleifer, R. Y. Rozen, *J. Am. Chem. Soc*. **2004**, *126*, 14850–14857.
40. H. Paloniemi, T. Aalritalo, T. Laiho, H. Liuke, N. Kocharova,K. Haapakka, F. Terzi, R. Seeber, J. Lukkari, *J. Phys. Chem. B* **2005**, *109*, 8634–8642.
41. M. J. O'Connell, P. Boul, L. M. Ericson, C. Huffman, Y. Wang, E. Haroz, C. Kuper, J. Tour, K. D. Ausman, R. E. Smalley, *Chem. Phys. Lett*. **2001**, *342*, 265–271.

42. M. S. Strano, V. C. Moore, M. K. Miller M. J. Allen, E. H. Haroz, C. J. Kittel, R. H. Hange, R. E. Smallez, *J. Nanosci. Nanotech*. **2003,** *3*, 81–86.
43. A. Star, Y. Liu, K. Grant, L. Ridvan, J. F. Stoddart, D. W. Steuerman, M. R. Diehl, A. Boukai, J. R. Heath, *Macromolecules* **2003**, *36 (3)*, 553–560.
44. E. Brosio, F. Conti, C. Lintas, S. Sykora, *J. Food Technol*. **1978,** *13*, 107–116.

Povzetek

V delu so predstavljeni rezultati sinteze in karakterizacije enostenskih ogljikovih nanocevk po funkcionalizaciji s hidroksietil celulozo. Lastnosti prvotnih in funkcionaliziranih ogljikovih nanocevk smo primerjali z različnimi metodami: termogravimetrično analizo, Ramansko spektroskopijo, FTIR spektroskopijo in UV-VIS-NIR spektrofotometrijo. Ramanska spektroskopska analiza je pokazala, da je za funkcionalizacijo kovinskih enostenskih ogljikovih nanocevk potrebna manjša količina hidroksietil celuloze v primerjavi s polprevodnimi nanocevkami. FTIR spektroskopska analiza je potrdila prisotnost hidroksietilnih skupin, kar dokazuje funkcionalizacijo nanocevk.